PAMUKKALE ÜNİVERSİTESİ
Mühendislik Bilimleri Dergisi

Araştırma makalesi | Research paper

PAMUKKALE UNIVERSITY
Journal of Engineering Sciences

Cilt | Vol: XX • Sayı | No: X • ss | pp: XXXX-XXXX • Yıl | Year: 20XX

Electrochemical impedance spectroscopy analysis of electrodeposited WO_3 thin films under dark and illuminated conditions

Sinem Kartal, Ece Değirmenci, Gamze Atak

ARTICLE INFO

Dates:
Received: 30.04.2026
Accepted: 10.09.2026

Doi:
10.65206/pajes.1940800

Corresponding author:
Gamze Atak
(gbaser@hacettepe.edu.tr)

Author addresses:
Department of Physics Engineering, Hacettepe University, Ankara, 06800, Türkiye
(sinemkartall20@gmail.com; ecedegirmenci@hacettepe.edu.tr; gbaser@hacettepe.edu.tr)

ABSTRACT

Context—Tungsten oxide (WO_3) is widely recognized as a promising material for photoelectrochemical applications due to its favorable optical transparency, chemical stability, and suitable band gap. Understanding the relationship between deposition parameters and interfacial charge transfer behavior is essential for improving the performance of WO_3-based devices.

Objective—In this study, tungsten oxide (WO_3) thin films were deposited on FTO-coated glass substrates at −0.6 V and −0.7 V using a potentiostatic electrodeposition technique. The effect of deposition potential on surface morphology, optical properties, and photoelectrochemical behavior was systematically investigated.

Method—SEM analysis revealed that both films exhibit homogeneous and continuous structures, while the sample deposited at −0.7 V shows more pronounced agglomeration, indicating enhanced nucleation and growth kinetics at higher deposition potentials. UV–Vis measurements demonstrated that both samples exhibit high optical transmittance in the visible region (approximately 70–80%), whereas a slight decrease was observed for the −0.7 V sample due to increased light scattering associated with higher surface roughness. Electrochemical Impedance Spectroscopy (EIS) and Photoelectrochemical Impedance Spectroscopy (PEIS) measurements were carried out under dark conditions, as well as under 535 nm monochromatic and Xe lamp illumination. The impedance data was further analyzed using equivalent circuit modeling to evaluate interfacial parameters such as charge transfer resistance and capacitive behavior.

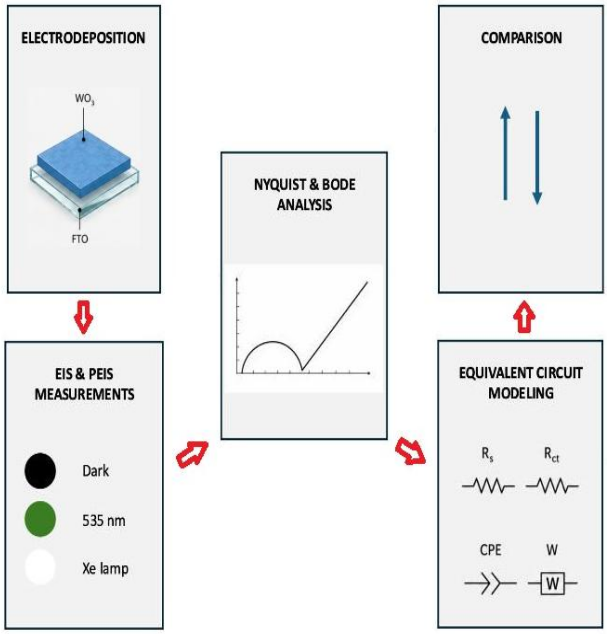

Results—While predominantly capacitive behavior was observed under dark conditions, a significant decrease in impedance under illumination indicates the generation of photo-induced charge carriers and enhanced interfacial charge transfer processes. Comparative analysis showed that the sample deposited at −0.6 V exhibits lower impedance and a more stable interfacial response under illumination, indicating more efficient charge transfer. In contrast, the sample deposited at −0.7 V demonstrates a more complex impedance response associated with increased surface heterogeneity and recombination processes.

Conclusion—These results demonstrate that the deposition potential plays a decisive role in determining the interfacial kinetics and electrochemical behavior of WO_3 thin films, and that a potential of −0.6 V enables more efficient charge transfer. These findings highlight the critical role of deposition parameter optimization in tailoring the interfacial properties of WO_3 thin films. This study positions EIS and PEIS techniques as indispensable characterization tools for advancing WO_3-based photoelectrochemical systems and provides a strong foundation for the design of next-generation smart window technologies and efficient solar-driven hydrogen production systems.

Key Words—Electrochemical impedance spectroscopy (EIS), Electrodeposition, Photoelectrochemical impedance spectroscopy (PEIS), Thin film, Tungsten oxide.

I. INTRODUCTION

Tungsten oxide (WO_3) is an n-type semiconductor with a wide range of applications, including electrochromic devices, gas sensors, and photoelectrochemical systems [1]-[6]. It holds an important place among advanced functional materials due to the tunability of its optical and electrochemical properties [7]–[9]. WO_3 thin films are widely used in smart window technologies because of their ability to interact with visible light and their chemical stability [10]–[12]. Electrochromic WO_3-based systems enable the control of optical properties (transmittance, reflectance and absorbance) through an applied potential, thereby playing a critical role in the development of energy-efficient buildings called as smart windows [7], [11]. In recent years, studies focusing on performance enhancement through doped WO_3 films and nanocomposite structures have gained increasing attention, and it has been demonstrated that the light modulation capability and cycling stability of these systems can be significantly improved [10]–[12]. WO_3 exhibits a monoclinic crystal structure at room temperature, which is the most stable phase, with reported optical band gap values typically around 2.6–2.8 eV for crystalline structures, although higher values (up to ~3.4 eV) have been reported depending on the film structure and preparation conditions [8], [13], [14]. Despite these favorable properties, WO_3-based systems are often limited by rapid surface recombination and insufficient visible light absorption, which restrict their overall photoelectrochemical performance [15], [16].

Beyond electrochromic applications, WO_3 also emerges as a prominent photoanode material in photoelectrochemical (PEC) water splitting processes [15], [17], [18]. The increasing global energy demand and the serious environmental problems caused by fossil fuel-based carbon emissions have intensified the need for sustainable energy technologies [13], [19], [20]. In this context, PEC water splitting systems, which directly convert solar energy into chemical energy, are considered one of the most effective approaches for carbon-neutral hydrogen production [21]. WO_3 is frequently preferred in PEC systems due to its favorable electronic properties, high chemical stability, and low cost, and performance improvements have been reported particularly through heterostructures and nanostructured electrodes [15], [17], [18], [22].

Among the various fabrication techniques employed for WO_3 thin films, including sputtering, sol-gel processing, chemical vapor deposition, and thermal evaporation, electrodeposition has attracted considerable attention due to its low equipment cost, scalability, low-temperature processing, and precise control over film thickness and morphology. Furthermore, the electrochemical growth process allows direct tuning of microstructural properties through deposition parameters such as potential and deposition time. However, in WO_3-based systems, charge carrier recombination, interfacial kinetics, and mass transport processes are among the main factors limiting system performance [15], [17]. A detailed understanding of these processes is critical not only for material optimization but also for improving device performance. At this point, Electrochemical Impedance Spectroscopy (EIS), which can analyze dynamic processes occurring at the electrode/electrolyte interface in a frequency-dependent manner, stands out as a powerful and non-destructive characterization technique [23]. EIS provides detailed information about the electrochemical behavior of the system by separating parameters such as charge transfer resistance, double-layer capacitance, and diffusion processes through equivalent circuit models [23]-[25].

In photoelectrochemical systems, Photoelectrochemical Impedance Spectroscopy (PEIS) is used to directly investigate the effect of light [26], [27]. PEIS measurements enable the separation of processes such as the generation, transport, and recombination of photo-generated electron–hole pairs in semiconductor electrodes, providing significant advantages especially in determining surface states and interfacial kinetics [24], [28]. In the literature, PEIS studies conducted on WO_3 and similar photoanode materials have shown that system behavior under illumination differs significantly from that under dark conditions and that additional time constants emerge [28]-[30].

The novelty of this study lies in the systematic comparison of the impedance response of WO_3 thin films prepared by electrodeposition under different illumination conditions. While most studies mainly focus on broadband illumination, in this work, EIS and PEIS measurements were carried out under three distinct conditions: dark, 535 nm monochromatic LED, and Xe lamp illumination. Furthermore, by analyzing samples prepared at different deposition potentials (−0.6 V and −0.7 V) with controlled and comparable thicknesses (~380 nm), the effect of thickness was minimized, allowing a direct evaluation of the influence of deposition parameters and illumination conditions on interfacial kinetics. This approach provides a clearer understanding of the fundamental mechanisms governing the performance of WO_3-based photoanode systems.

II. EXPERIMENTAL TECHNIQUES and PROCEDURES

A. Film Deposition

Sodium tungstate dihydrate ($Na_2WO_4.2H_2O$), hydrogen peroxide solution (H_2O_2, 30 wt.% in H_2O), perchloric acid ($HClO_4$, 60%) were purchased from Sigma-Aldrich. Fluorine-doped tin oxide (FTO) containing glass was purchased from Teknoma Technological Materials Industrial and Trading Inc.

WO_3 thin films were deposited on FTO-coated glass substrates using a potentiostatically controlled electrodeposition technique. Before deposition, FTO coated glass substrates were cleaned with acetone (10 min), ethanol (10 min), and DI water (10 min) under ultrasonication. A conventional three-electrode electrochemical system was employed as shown in Fig. 1, where the FTO substrate served as the working electrode (WE), a platinum (Pt) wire was used as the counter electrode (CE), and an Ag/AgCl electrode was used as the reference electrode (RE).

For the deposition of the film, the solution was prepared by dissolving 1.03 g of $Na_2WO_42H_2O$ in 125 mL of DI water, and then 0.65 mL of H_2O_2 was added under magnetic stirring with 600 rpm. Adding $HClO_4$ (60%) adjusted the pH to 1.0-1.2 and continue stirring with 600 rpm at 30 min. After electrodeposition, the samples were washed with DI water and dried in air. The films were deposited by applying constant potentials of −0.6 V and −0.7 V using an electrodeposition technique.

Potentiostatic depositioninitiated by a potential step was preferred because the applied potential directly controls the electrochemical reduction kinetics of tungsten species. Maintaining a constant potential provides stable growth

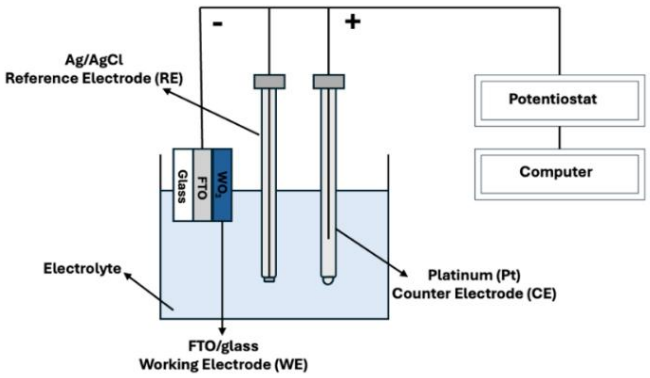

Fig. 1. Schematic representation of the three-electrode electrochemical setup employed for the electrodeposition of WO_3 thin films.

conditions and enables a direct evaluation of the influence of deposition potential on film morphology and electrochemical behavior.

B. Sample characterization

The thickness, structure, morphology and optical properties of the films were characterized with the instruments described below.

Film thickness was recorded by surface profilometry using a Bruker DektakXT instrument and was approximately 380 nm. X-ray diffraction (XRD) analysis was performed using a Rigaku Ultima-IV diffractometer with CuKα radiation, operating at a wavelength of 1.5406 Å, 40 kV, and 30 mA, for diffraction angles of $20° \leq 2\theta \leq 80°$ with steps of 0.02° for structural characterization. The morphology and compositional study of the films was studied by scanning electron microscopy (SEM) using a FEI Quanta 200 FEG instrument with an acceleration voltage of 30 kV and energy dispersive X-ray spectroscopy (EDX).

The optical transmittance ($T(\lambda)$) spectra of the as-deposited film and FTO coated glass substrate were measured by using a Cary 5000 UV-Vis-NiR spectrophotometer in the range of 250-1200 nm. The optical absorption coefficient (α) was obtained from the optical density expression by using Beer-Lambert's law [31], as in (1) and (2):

$$I = I_0 e^{-\alpha d}, \quad (1)$$

$$OD = -\log_{10}(I/I_0) = \alpha d/\log_e(10) = 0.434\alpha d, \quad (2)$$

where OD and d denote optical density and film thickness, respectively.

The optical band gap (E_g) values were determined from the obtained absorbance data using the Tauc plot method.

The techniques described so far characterize the films themselves. The electrochemical behaviour of the electrodes was measured separately, in a three-electrode cell. EIS and PEIS measurements were carried out using a conventional three-electrode electrochemical cell, as illustrated in Fig. 2. The WO_3-coated FTO substrate was used as the working electrode (WE), a platinum (Pt) electrode served as the counter electrode (CE), and an Ag/AgCl electrode was employed as the reference electrode (RE). The electrolyte solution consisted of 0.5 M H_2SO_4. A 0.5 M H_2SO_4 electrolyte was selected because WO_3 exhibits good electrochemical stability in acidic media and sulfuric acid is widely employed in photoelectrochemical studies of WO_3-based electrodes due to its high ionic conductivity and well-established electrochemical behavior. EIS measurements were performed under dark conditions, while PEIS measurements were conducted under two different illumination conditions: 535 nm monochromatic green light and Xe lamp illumination simulating broadband solar radiation. The Xe lamp intensity was adjusted to approximately 1000–1200 W/m^2, while the green light intensity was set to approximately 35 W/m^2 for the investigated samples.

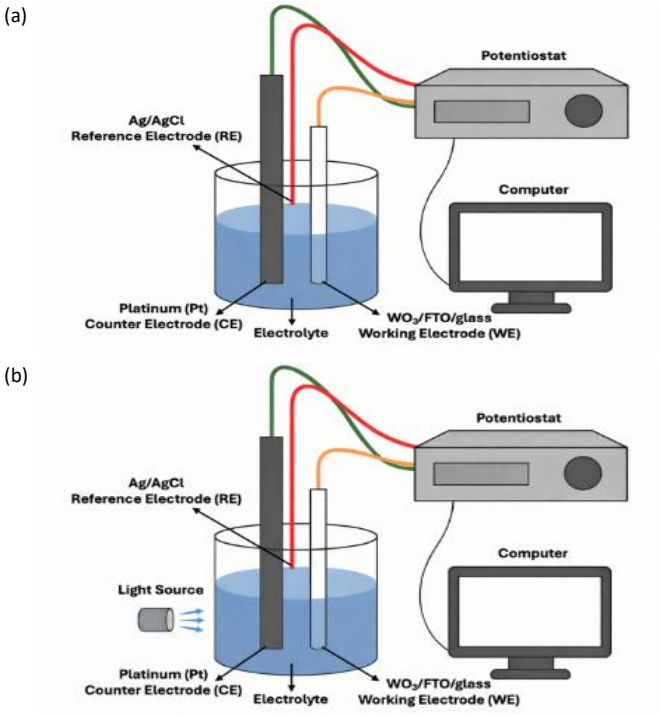

Fig. 2. Schematic illustration of the electrochemical measurement setup used for (a) EIS measurements under dark conditions and (b) PEIS measurements under illumination.

All impedance measurements were carried out at a DC potential of 0 V vs. OCP, with an AC perturbation amplitude of 10 mV. The frequency range was swept from 10 kHz to 0.01 Hz to analyze both high-frequency interfacial processes and low-frequency diffusion-controlled processes. The obtained impedance data were analyzed using equivalent circuit models. The fitting procedures were performed using Corrtest electrochemical analysis software, and the ability of the models to represent the experimental data was evaluated.

III. RESULTS and DISCUSSION

A. Film growth, morphology and optical properties

This section first covers how the films deposited during deposition and what their structure, morphology and optical properties are. The impedance response measured in the dark and under illumination is then discussed together with these properties.

The electrodeposition process was monitored in situ by recording current density–time (J–t) curves, as shown in Fig. 3. Figs. 3a and 3b present the current responses obtained at −0.6 V and −0.7 V, respectively, over a deposition period of 1800 s. Both samples exhibit stable current responses throughout the deposition process, indicating a controlled nucleation and growth mechanism [9], [16]. The initial transient region corresponds to the nucleation stage, followed by a quasi-steady regime associated with continuous film growth. The transient positive current excursions observed in the current-time curves are attributed to charging/discharging processes of the electrical double layer and potentiostat stabilization effects during data acquisition. These short-duration positive responses do not indicate film dissolution but rather reflect transient interfacial processes superimposed on the overall cathodic deposition current. A comparison of the two samples shows that the film deposited at −0.7 V exhibits slightly higher absolute current densities (≈ −15 mA cm^{-2}) compared to the −0.6 V sample (≈ −14 mA cm^{-2}), as observed from the peak values in the J–t curves. This behavior can be attributed to the increased driving force for the reduction of tungsten species at more negative potentials, which enhances the nucleation kinetics and influences the resulting film morphology.

Figs. 3c and 3d show enlarged views of the initial region, further confirming the rapid current transitions during deposition. In addition, the gradual increase in the current envelope suggests an increase in electroactive surface area as the WO_3 layer grows. The J–t curves describe how the films were formed but say nothing about the structure that resulted. XRD measurements were therefore carried out on both samples.

Fig. 4 shows the XRD pattern of WO_3 film on FTO coated glass substrate with 0.7° grazing angle. XRD pattern showed that the films were amorphous. The diffraction peaks observed in the XRD pattern can be attributed to the FTO-coated glass substrate (JCPDS No. 46-1088).

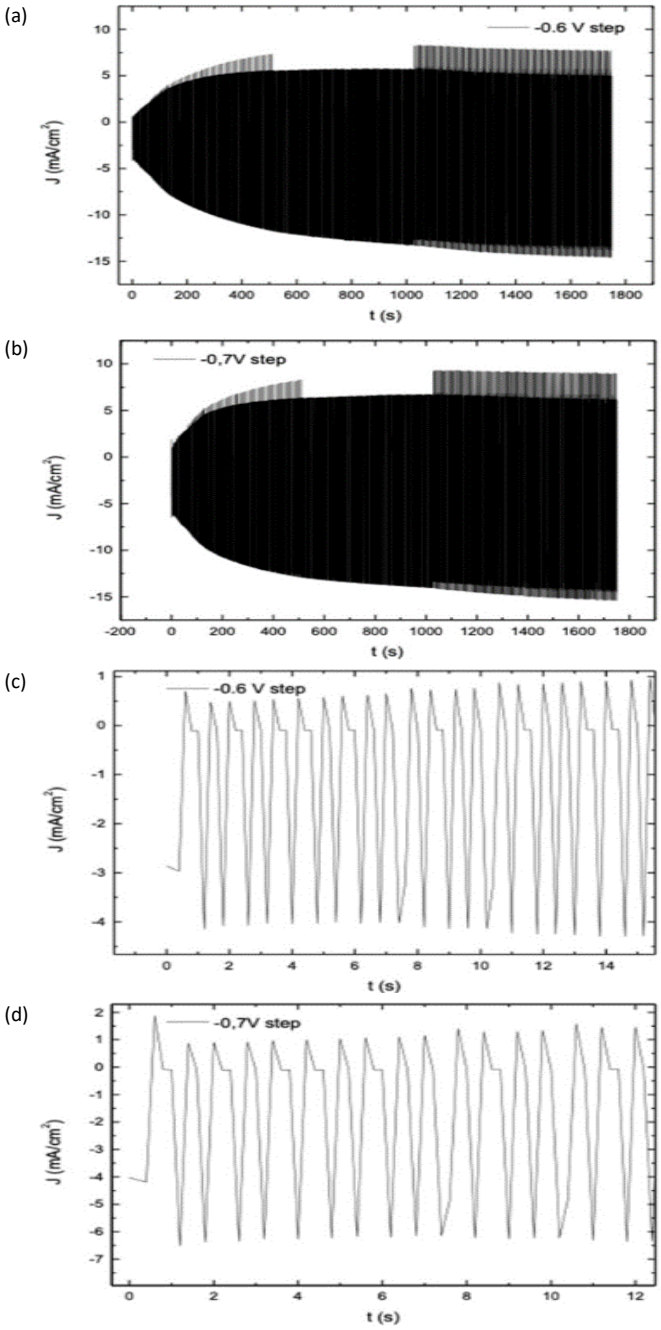

Fig. 3. Current density–time (J–t) curves of WO_3 thin films electrodeposited at (a) −0.6 V and (b) −0.7 V, together with enlarged views of the initial deposition stage for (c) −0.6 V and (d) −0.7 V.

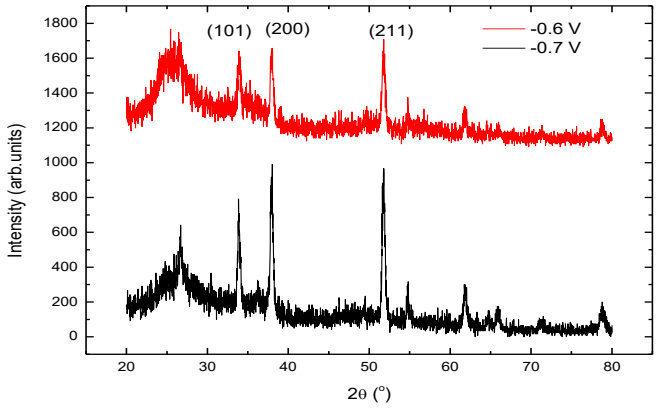

Fig. 4. XRD patterns of potansiostatic electrodeposited WO_3 films with -0.6V and -0.7V potential on FTO coated glass substrates. The observed diffraction peaks originate from the FTO-coated substrate (JCPDS No. 46-1088).

Since neither film is crystalline, any difference between them must come from the way the material is arranged on the surface. This was examined by SEM.

Surface morphology is one of the key factors determining the electrochemically active area of photoelectrodes and their interaction with the electrolyte interface, directly influencing charge transfer processes [32]. In electrodeposited WO_3 systems, the applied potential governs nucleation and growth kinetics, thereby controlling the resulting nanostructure and surface properties [33].

As shown in Figs. 5a and 5b, both samples exhibit homogeneous and continuous film structures characteristic of the electrodeposition method. However, the sample deposited at −0.7 V shows larger and more pronounced agglomerates. This behavior can be attributed to accelerated nucleation and particle coalescence under higher overpotential conditions [34].

In addition to SEM measurements, EDX analyses were performed to determine the elemental distribution on the surface. Due to the high energy and penetration depth of the incident X-rays, elements originating from the substrate (FTO-coated glass, soda–lime glass), such as Si, Ca, and Na, were also detected. Besides these substrate-related elements, W, O, Na, and Cl were identified in the films. The presence of Na is attributed to the alkaline precursor salt ($Na_2WO_4{\cdot}2H_2O$) used during the film growth process, while Cl originates from $HClO_4$ added to the electrolyte for pH adjustment.

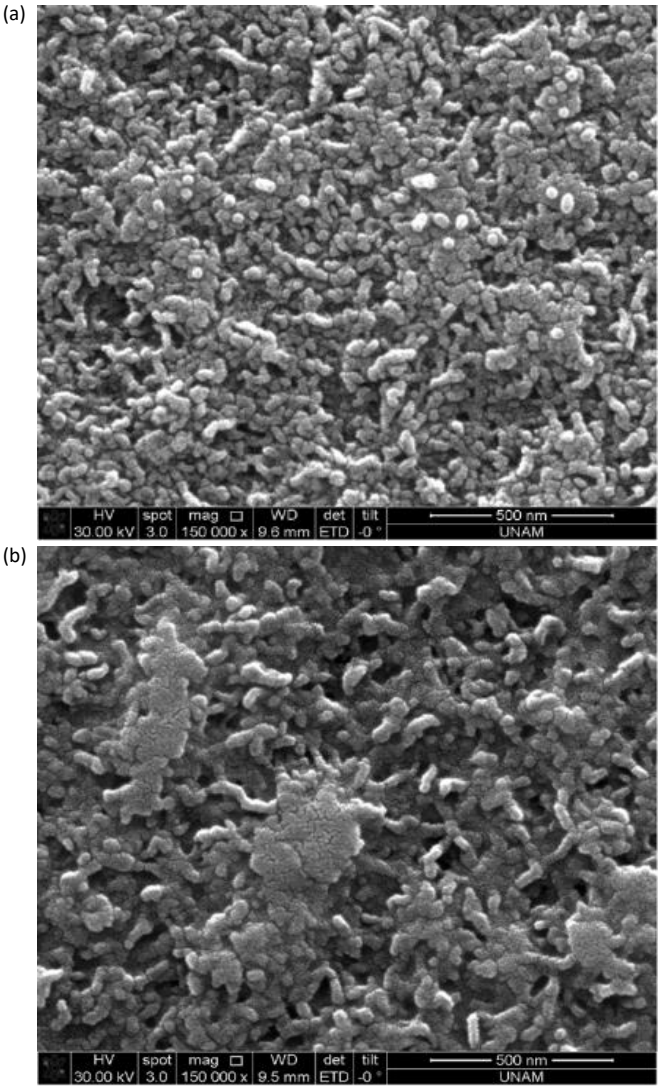

Fig. 5. Top-view SEM images of WO_3 thin films deposited at (a) −0.6 V and (b) −0.7 V.

Profilometry gave nearly the same thickness for both films, about 380 nm. The two samples can therefore be compared directly, and the differences described above come from the deposition potential rather than from a difference in thickness. Therefore, the observed morphological differences can be attributed primarily to the deposition parameters.

The surface features seen in SEM also change how light passes through the films, so the optical response was measured next. The transmittance spectra are given in Fig. 6. Both samples exhibit a sharp absorption edge in the range of 370–380 nm, which is consistent with the characteristic band gap behavior of WO_3 thin films [33]. In the visible region, the films show high transmittance values (approximately 70–80%), indicating good optical transparency. A slight decrease in transmittance is observed for the −0.7 V sample, which can be attributed to increased surface roughness and enhanced light scattering, consistent with the SEM observations.

The absorption edge gives a rough idea of the band gap, but a value can be read properly from Tauc plots. These are shown in Fig. 7.

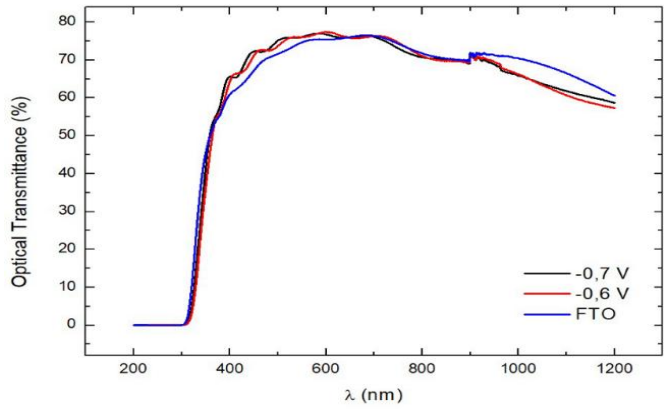

Fig. 6. Optical transmittance spectra of WO_3 thin films electrodeposited at −0.6 V and −0.7 V, together with the FTO substrate as a reference.

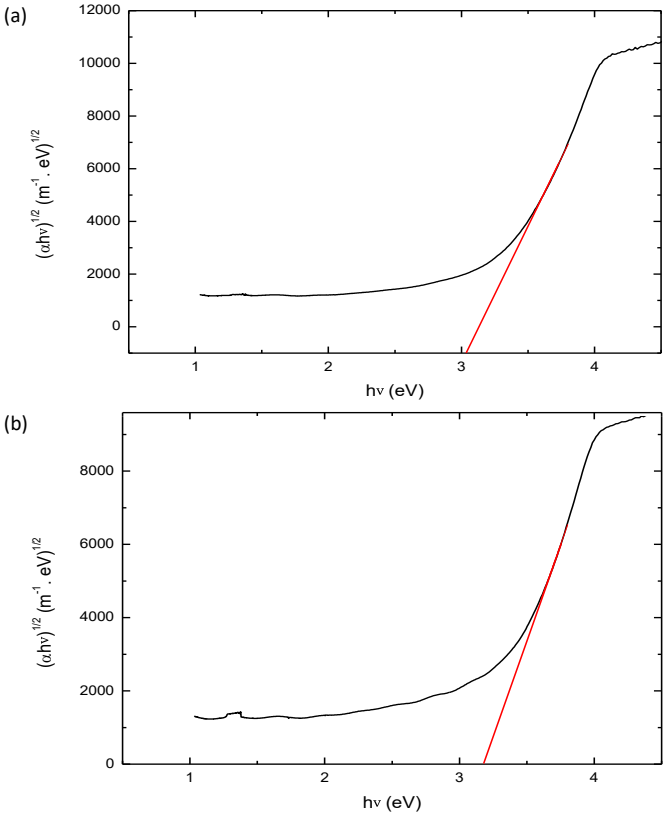

Fig. 7. Tauc plots of WO_3 thin films electrodeposited at (a) −0.6 V, (b) −0.7 V.

The band gap is 3.12 eV for the film deposited at −0.6 V and 3.17 eV for the film deposited at −0.7 V. Both values lie somewhat below the 3.26–3.35 eV estimated directly from the absorption edge at 370–380 nm, which is expected since the linear extrapolation leaves out the band tail.

The measured gaps of 3.12 and 3.17 eV exceed the 2.6–3.0 eV range normally quoted for crystalline monoclinic WO_3 [8], [14]. The reason is the amorphous and hydrated nature of films deposited from aqueous peroxotungstate electrolytes, which is confirmed by the XRD pattern in Fig. 4. Wider gaps of the same kind have been measured for $WO_3 \cdot xH_2O$ and for amorphous WO_3 layers, where structural disorder and retained water shift the absorption edge to higher energy [35]-[39]. Our values therefore sit where one would expect for electrodeposited films used without any post-deposition heat treatment.

Overall, the results indicate that both samples exhibit similar thickness and optical properties, while the deposition potential plays a critical role in determining surface morphology, which in turn directly influences light–matter interaction and is expected to impact the electrochemical and photoelectrochemical response of the films. All of these measurements describe the films on their own. How they behave once they are in contact with the electrolyte is a separate question, and this is what the impedance measurements address.

B. Electrochemical impedance analysis under dark conditions

EIS measurements were performed to investigate the interfacial charge transfer processes and electrochemical behavior of WO_3 thin films under dark conditions. The Nyquist plots (Fig. 8) and the Bode plots (Fig. 9) enable a direct comparison of the impedance responses of the samples electrodeposited at −0.6 V and −0.7 V. The Nyquist plots provide insight into charge transfer resistance and capacitive behavior at the electrode/electrolyte interface, while the Bode plots allow evaluation of frequency-dependent impedance magnitude and phase angle, offering additional information about the dominant electrochemical processes [23], [24]. Although a common equivalent circuit model was evaluated for both samples, the impedance response of the film deposited at −0.7 V could not be satisfactorily represented using the simpler model employed for the −0.6 V sample. Therefore, different equivalent circuits were selected to achieve physically meaningful fitting parameters and lower fitting errors.

R_S represents the uncompensated solution resistance, R_{ct} corresponds to the charge-transfer resistance at the electrode/electrolyte interface, CPE elements account for non-ideal capacitive behavior arising from surface roughness and heterogeneity, and L represents inductive contributions that may originate from wiring effects or rapid interfacial relaxation processes.

As shown in Fig. 8, both samples exhibit a high impedance response over a wide frequency range and display a nearly vertical trend in the Nyquist plots. This behavior indicates a dominant capacitive response rather than a well-defined semicircle associated with charge transfer processes. Under dark conditions, the absence of photo-generated charge carriers limits charge transfer mechanisms, leading the system to be governed primarily by double-layer capacitive behavior, which is represented by constant phase elements (CPEs) [23], [24].

The sample deposited at −0.7 V exhibits a steeper impedance response, indicating a stronger capacitive character. This behavior can be attributed to the increased effective surface area associated with the larger agglomerates observed in the SEM analysis. In contrast, the slight deviation observed for the −0.6 V sample suggests that charge transfer processes may still contribute to the overall response, even under dark conditions.

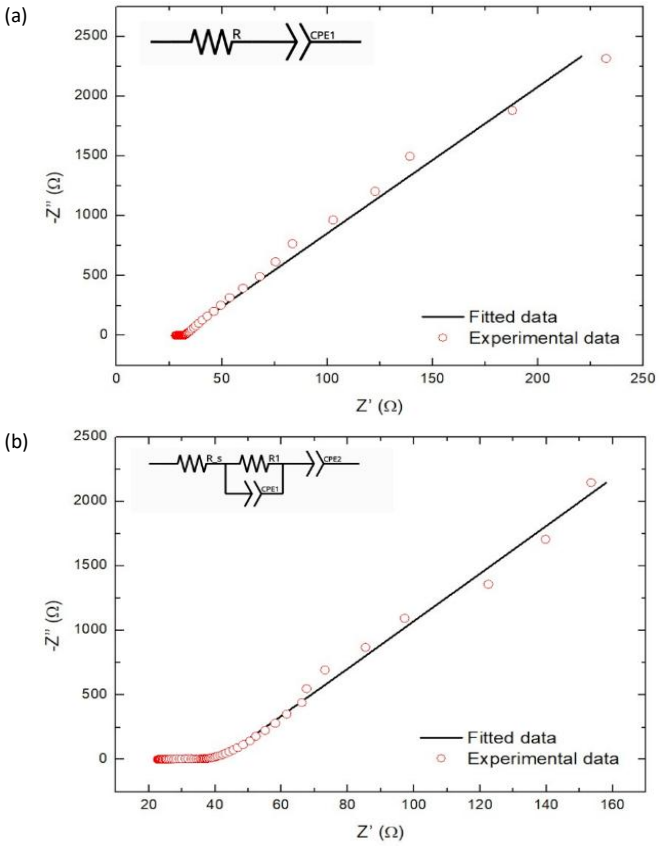

Fig. 8. Nyquist plots of WO_3 thin films electrodeposited under dark conditions, together with the corresponding equivalent circuit models used for fitting: (a) film deposited at −0.6 V and (b) film deposited at −0.7 V.

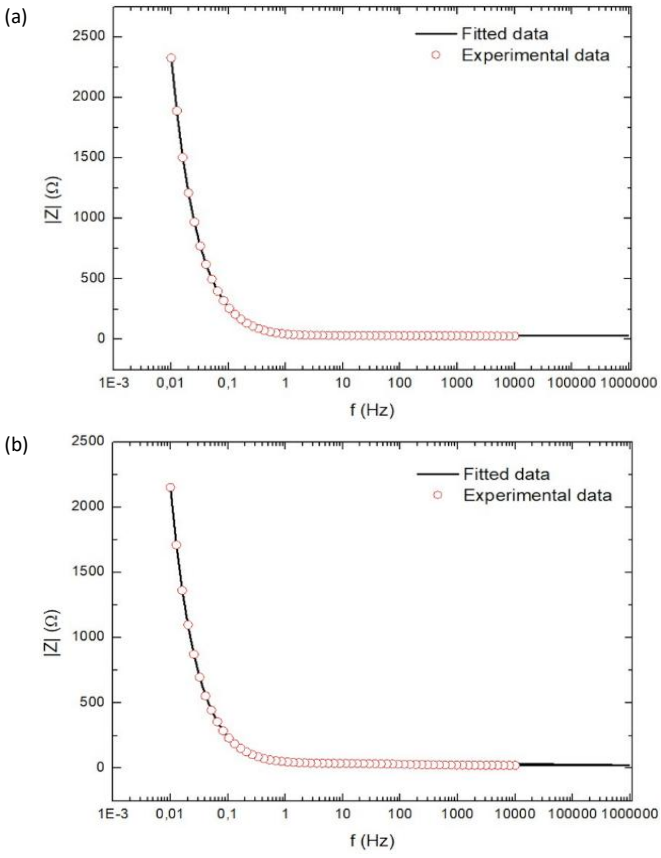

Fig. 9. Bode plots of WO_3 thin films electrodeposited under dark conditions: (a) film deposited at −0.6 V and (b) film deposited at −0.7 V.

The Bode plots further support these observations. The significant increase in impedance magnitude at low frequencies, reaching approximately 10^3 Ω, confirms the highly resistive nature of the system under dark conditions. Additionally, the phase angle approaching −90° in this region indicates dominant capacitive behavior [23, 24]. At higher frequencies, the stabilization of impedance and the decrease in phase angle reveal the increasing contribution of resistive elements. The strong agreement between Nyquist and Bode analyses confirms that the selected equivalent circuit model reliably represents the system.

The fitting results indicate that a simpler equivalent circuit model (Fig. 8a) is sufficient to describe the −0.6 V sample, whereas a more complex model (Fig. 8b) is required for the −0.7 V sample. This difference suggests a more heterogeneous and structurally complex interfacial behavior for the latter. As summarized in Table 1, the −0.7 V sample exhibits a lower series resistance (R_S = 20.9 Ω) compared to the −0.6 V sample (R_S = 30.4 Ω), which may indicate improved charge transport characteristics at the electrode/electrolyte interface. Furthermore, the p_CPE2 value of 0.966 suggests behavior close to that of an ideal capacitor, indicating a highly capacitive interface.

The relatively low RMSE values (2.4% and 4.5%) confirm the good agreement between the experimental data and the fitted models, supporting the validity of the selected equivalent circuits. The more advanced equivalent circuit used for the −0.7 V sample (Fig. 8b) reflects increased surface heterogeneity and possible porous or distributed structures, which is in strong agreement with the SEM observations of larger agglomerates. The absence of additional circuit elements for the −0.6 V sample further supports its simpler and more homogeneous interfacial structure. The dark measurements show what the interface does in the absence of photogenerated carriers. The same measurements were then repeated under illumination to see the effect of light.

C. Photoelectrochemical impedance analysis under 535 nm illumination

PEIS measurements were performed under 535 nm monochromatic illumination to investigate the photo-induced charge transfer processes and interfacial behavior of WO_3 thin films. The EIS measurements were carried out under illumination at 535 nm, corresponding to a photon energy of 2.36 eV. This energy is lower than the optical band gap values determined for the films deposited at −0.6 V (3.13 eV) and −0.7 V (3.17 eV). Therefore, direct band-to-band excitation is not expected under these conditions. The observed photoelectrochemical response may instead originate from defect-related electronic states and band-tail absorption associated with the amorphous WO_3 structure. The Nyquist plots (Fig. 10) and the Bode plots (Fig. 11) enable a direct comparison of the impedance responses of the samples electrodeposited at −0.6 V and −0.7 V under green light illumination. The Nyquist plots provide information on the charge transfer resistance and capacitive behavior at the electrode/electrolyte interface under illumination, while the Bode plots allow evaluation of the frequency-dependent impedance magnitude and phase angle, offering further insight into the photoelectrochemical processes [24].

As shown in Fig. 10, both samples maintain a predominantly capacitive behavior under 535 nm illumination; however, a significant decrease in impedance magnitude (|Z|) is observed compared to the dark condition (Fig. 8). This suggests that incident light generates electron–hole pairs within the WO_3 structure, thereby enhancing charge transfer processes at the electrode/electrolyte interface [24], [28].

The sample deposited at −0.7 V exhibits a steeper impedance response, indicating a more pronounced capacitive character under illumination. This behavior is consistent with the increased surface heterogeneity observed in the SEM analysis. In contrast, the −0.6 V sample shows lower impedance values, suggesting more efficient light-induced charge transfer processes.

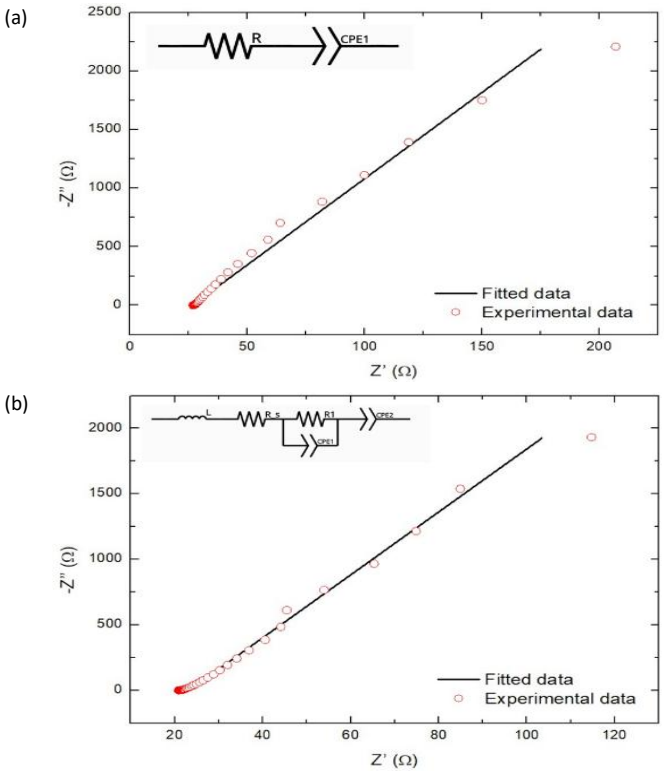

Fig. 10. Nyquist plots of WO_3 thin films electrodeposited under 535 nm monochromatic illumination, together with the corresponding equivalent circuit models used for fitting: (a) film deposited at −0.6 V and (b) film deposited at −0.7 V.

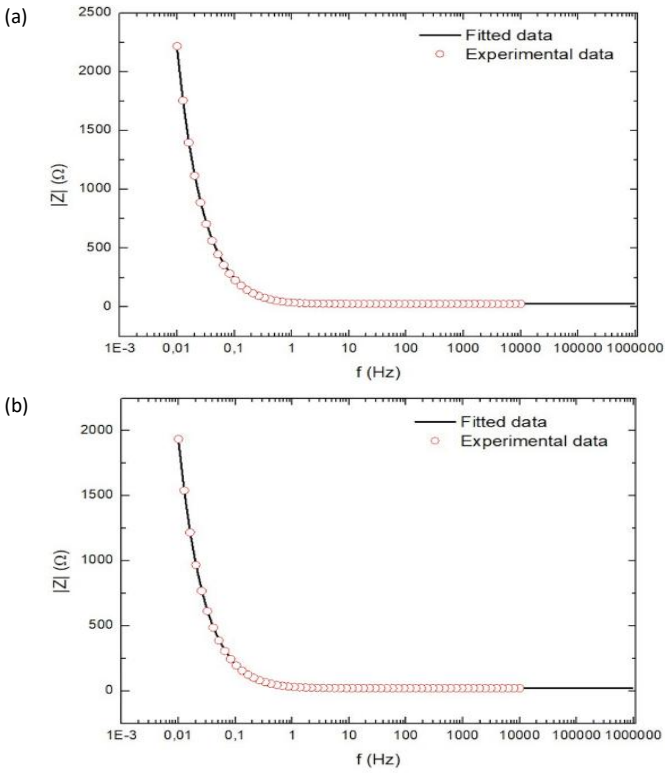

Fig. 11. Bode plots of WO_3 thin films electrodeposited under 535 nm monochromatic illumination: (a) film deposited at −0.6 V and (b) film deposited at −0.7 V.

The Bode plots further support these findings. A clear decrease in impedance magnitude at low frequencies is observed under illumination, reflecting reduced interfacial resistance and increased carrier density [24]. The shift in phase angle indicates a transition from ideal capacitive behavior toward a regime influenced by charge transfer kinetics [23].

At higher frequencies, the impedance tends to stabilize, confirming the dominance of the series resistance (R_S) [23]. Notably, the equivalent circuit used for the −0.7 V sample includes an inductance (L) element, which accounts for the inductive behavior observed at high frequencies. Such inductive contributions are often associated with measurement artifacts such as wiring effects or contact resistances, although they may also reflect fast interfacial processes [23]. Their inclusion improves the overall fitting accuracy of the model.

As summarized in Table 1, the −0.7 V sample exhibits a significantly reduced charge transfer resistance ($R_1 \approx 2.41\ \Omega$), indicating enhanced interfacial charge transfer kinetics under illumination. In contrast, the −0.6 V sample can be well described by a simpler equivalent circuit, reflecting a more dominant capacitive response. Furthermore, the p_CPE values approaching unity (0.957 and 0.974) are indicative of near-ideal capacitive behavior for both samples under illumination. The presence of multiple CPE elements and an inductive contribution in the −0.7 V sample suggests a more complex and heterogeneous interfacial response involving multiple time constants. The low RMSE values (1.8% and 3.1%) confirm the reliability andaccuracy of the equivalent circuit fitting, demonstrating strong agreement between the experimental data and the proposed models. Monochromatic light at 535 nm excites only part of the absorption range of WO_3. A Xe lamp was used next so that the films could be compared under broadband illumination.

D. Photoelectrochemical impedance analysis under Xe lamp illumination

PEIS measurements were performed under Xe lamp illumination to investigate the photo-induced charge transfer processes and interfacial behavior of WO_3 thin films under broadband light conditions. The Nyquist plots (Fig. 12) and the Bode plots (Fig. 13) enable a direct comparison of the impedance responses of the samples electrodeposited at −0.6 V and −0.7 V under Xe lamp illumination.

The Nyquist plots provide information on the charge transfer resistance and capacitive behavior at the electrode/electrolyte interface under broadband illumination, while the Bode plots allow evaluation of the frequency-dependent impedance magnitude and phase angle, offering further insight into the photoelectrochemical processes [24]. As shown in Fig. 12, both samples maintain a predominantly capacitive behavior under Xe lamp illumination; however, more pronounced changes in impedance magnitude (|Z|) are observed compared to the 535 nm condition (Fig. 10). This suggests that incident broadband illumination generates a higher density of photo-induced charge carriers within the WO_3 structure [24], [28]. For the sample deposited at −0.7 V, the charge transfer resistance (R_1) increases to approximately 5.80 Ω. This increase suggests that, despite enhanced carrier generation, interfacial recombination processes and kinetic limitations may become more significant under high photon flux conditions [23]. Additionally, the lower p_CPE1 value indicates a deviation from ideal capacitive behavior, pointing to increased surface heterogeneity and the possible contribution of diffusion-related processes at low frequencies [23]. In contrast, the −0.6 V sample exhibits lower impedance values and can be described using a simpler equivalent circuit, indicating a less complex interfacial response under broadband illumination. The Bode plots further support these observations. A decrease in impedance magnitude at low frequencies confirms improved charge transport under illumination [24], while the high-frequency plateau corresponds to the dominance of the series resistance (R_S) [23]. The phase angle behavior reveals a deviation from ideal capacitive response, indicating the contribution of charge transfer kinetics and possible diffusion processes [23].

As summarized in Table 1, the series resistance ($R_S \approx 21.0\ \Omega$) of the −0.7 V sample remains relatively stable under different

Table 1. Equivalent circuit parameters obtained from EIS/PEIS measurements under dark, 535 nm monochromatic, and Xe lamp illumination for WO_3 thin films electrodeposited at −0.6 V and −0.7 V.

Condition	Sample (V)	R_S (Ω)	R_1 (Ω)	p_CPE1	T_CPE1	p_CPE2	T_CPE2	RMSE	Norm. RMSE (%)
Dark	−0.7	20.9	21.5	0.495	0.00293	0.966	0.00674	2.4383	2.1207
Dark	−0.6	30.4	—	0.948	0.00589	—	—	4.5235	4.4013
535 nm	−0.7	20.9	2.41	0.767	0.0242	0.974	0.00768	2.9738	1.8591
535 nm	−0.6	26.5	—	0.957	0.00644	—	—	6.8352	3.1103
Xe lamp	−0.7	21.0	5.80	0.359	0.0180	0.970	0.00749	3.4372	1.9461
Xe lamp	−0.6	26.7	—	0.960	0.00680	—	—	5.9763	3.0555

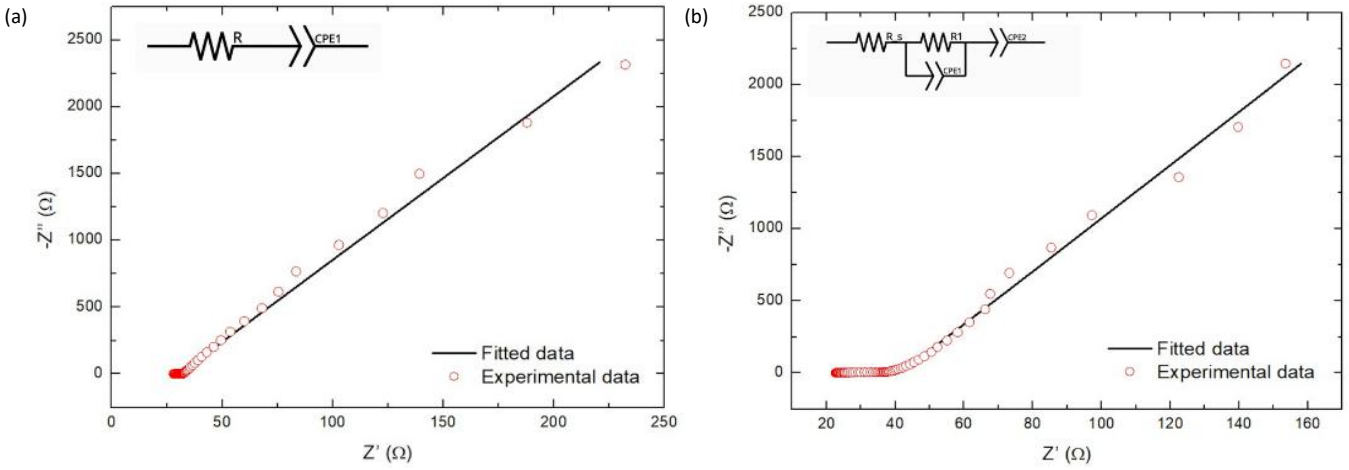

Fig. 12. Nyquist plots of WO_3 thin films electrodeposited under dark conditions, together with the corresponding equivalent circuit models used for fitting: (a) film deposited at −0.6 V and (b) film deposited at −0.7 V.

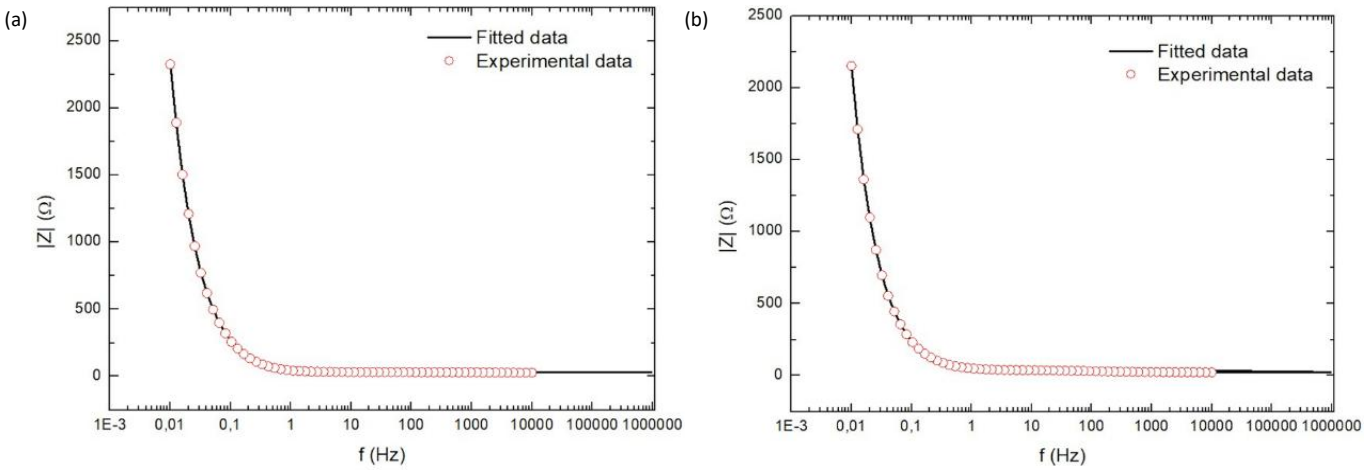

Fig. 13. Bode plots of WO_3 thin films electrodeposited under Xe lamp illumination (a) film deposited at −0.6 V and (b) film deposited at −0.7 V.

illumination conditions, indicating that the ohmic contribution is largely unaffected by light. The charge transfer resistance (R_1) of the −0.7 V sample increases compared to the 535 nm illumination condition, suggesting that although carrier generation is enhanced under broadband illumination, interfacial recombination processes and kinetic limitations become more significant. The low p_CPE1 value observed for the −0.7 V sample indicates a clear deviation from ideal capacitive behavior, reflecting increased surface heterogeneity and the contribution of more complex interfacial processes. In contrast, the −0.6 V sample maintains a p_CPE value closer to unity, indicating a more ideal capacitive response and a less complex interfacial structure. The low RMSE values (1.9% and 3.0%) confirm that the selected equivalent circuit models reliably represent the impedance behavior under Xe illumination, demonstrating strong agreement between the experimental data and the fitted models.

Taken together, the three illumination conditions show that the interfacial response of the films depends both on the deposition potential and on the amount of light reaching the electrode.

IV. CONCLUSION

In this study, WO_3 thin films were deposited with a step potential at −0.6 V and −0.7 V using an electrodeposition technique. The stable current density–time (J–t) responses obtained during deposition confirm that the nucleation and growth processes were well controlled under both applied potentials.

SEM analysis revealed that both samples exhibit homogeneous and continuous film structures, while the −0.7 V sample shows more pronounced agglomeration, reflecting increased surface heterogeneity at higher deposition potentials. UV–Vis measurements demonstrated that both films possess high optical transmittance in the visible region (70–80%) with comparable thicknesses (~380 nm). The slight decrease in transmittance observed for the −0.7 V sample can be attributed to enhanced light scattering caused by increased surface roughness.

EIS and PEIS results showed that both samples exhibit predominantly capacitive behavior under dark conditions, whereas a significant decrease in impedance was observed under

illumination. This behavior confirms the generation of photo-induced charge carriers and the enhancement of interfacial charge transfer processes under both 535 nm and Xe lamp illumination.

Comparative analysis revealed that the sample deposited at −0.6 V shows lower impedance and a more stable interfacial response under illumination, indicating more efficient charge transfer. In contrast, the −0.7 V sample shows an increase in charge transfer resistance under Xe lamp illumination, suggesting that recombination processes and interfacial kinetic limitations become more prominent due to increased surface heterogeneity.

Although the observed differences in impedance behavior are strongly influenced by surface morphology and interfacial area, intrinsic electronic properties of the WO_3 films also contribute to the measured response. Factors such as electronic conductivity, defect-state density, carrier transport characteristics, and localized electronic states can significantly affect charge-transfer kinetics and recombination processes. Therefore, the impedance behavior found in this study should be assessed as the combined result of both morphological and intrinsic electronic effects.

XRD analyses revealed that both films deposited at different potentials remained amorphous. Therefore, the observed differences in charge-transfer resistance cannot be attributed to variations in crystal structure. Instead, they are more likely related to potential-dependent changes in film morphology and microstructural features, which influence the interfacial charge-transfer process. Instead, SEM observations reveal that the film deposited at −0.7 V possesses a more porous and open morphology compared to the relatively compact structure obtained at −0.6 V. Such morphological differences are expected to affect the electrode/electrolyte interfacial area and charge-transfer kinetics, resulting in the observed variation in R_1 values.

Overall, the results demonstrate that the deposition potential plays a critical role in determining both the morphological structure and photoelectrochemical performance of WO_3 thin films. A deposition potential of −0.6 V provides a more favorable balance between surface morphology and charge transfer efficiency, making it a suitable parameter for the design of photoanodes in applications such as smart window technologies and solar-driven hydrogen production.

This study positions EIS and PEIS techniques as indispensable characterization tools for advancing WO_3-based photoelectrochemical systems by providing in-depth insight into interfacial charge transfer mechanisms. The findings not only emphasize the importance of impedance-based analysis in understanding electrochemical behavior but also establish a strong foundation for the rational design and optimization of next-generation smart window technologies and efficient solar-driven hydrogen production systems.

AUTHOR STATEMENT

Plagiarism Check—The article was scanned with iThenticate and found to be compliant with the journal's plagiarism policy.

Conflict of Interest—The authors declare that there is no conflict of interest regarding the publication of this article.

Ethics Committee Approval—Ethics committee approval is not required for this study. The authors declare that they comply with all applicable ethical standards.

Use of Artificial Intelligence Tools—AI was used only for grammar and language editing during the preparation of this article. All scientific content reflects the original contribution of the authors.

Funding—This study was supported by the Scientific and Technological Research Council of Türkiye (TÜBİTAK) under Project No. 223M337 and by the Hacettepe University Scientific Research Projects Coordination Unit under Project Nos. FHD-2024-21270 and FKB-2024-21248.

Data Availability—The main data supporting the findings of this work are available within the article.

CRediT Author Contribution—Investigation, Data Curation, Writing – Original Draft (**Sinem Kartal**); Investigation, Validation, Writing – Review & Editing (**Ece Değirmenci**); Conceptualization, Methodology, Investigation, Software, Visualization, Writing – Original Draft, Writing – Review & Editing, Supervision, Project Administration, Funding Acquisition (**Gamze Atak**).

Acknowledgment—The authors gratefully acknowledge METU Central Laboratory for the XRD measurements and Bilkent University National Nanotechnology Research Center (UNAM) for the UV–Vis–NIR and SEM measurements of the as-deposited samples.

REFERENCES

[1] F. H. An, Y. Z. Yuan, J. Q. Liu, M. D. He, B. Zhang, "Enhanced electrochromic properties of WO_3/ITO nanocomposite smart windows", *RSC Advances*, 13(19), 13177–13182, 2023. https://doi.org/10.1039/d3ra01428b.

[2] S. K. Deb, "Opportunities and challenges in science and technology of WO_3 for electrochromic and related applications", *Solar Energy Materials and Solar Cells*, 92(2), 245–258, 2008. https://doi.org/10.1016/j.solmat.2007.01.026.

[3] Y. N. Kanafin, A. Abduvalov, M. Kaikanov, S. G. Poulopoulos, T. Sh. Atabaev, "A review on WO_3 photocatalysis used for wastewater treatment and pesticide degradation", *Heliyon*, 11(1), e40788, 2025. https://doi.org/10.1016/j.heliyon.2024.e40788.

[4] M. Zhang, C. Yang, Z. Zhang, W. Tian, B. Hui, J. Zhang, K. Zhang, "Tungsten oxide polymorphs and their multifunctional applications", *Advances in Colloid and Interface Science*, 300, 102596, 2022. https://doi.org/10.1016/j.cis.2021.102596.

[5] H. Abbas, Z. Khaliq, N. Nadeem, M. B. Qadir, M. U. Rehman, D. Umer, Z. Jilani, M. W. Shahzad, "Recent advancements in WO_3-based polymeric nanocomposites for photocatalytic applications: a comprehensive review", *Chemical Papers*, 80(6), 5785-5827, 2026. https://doi.org/10.1007/s11696-026-04708-6.

[6] M. I. Nabeel, D. Hussain, N. Ahmad, M. Najam-ul-Haq, S. G. Musharraf, "Recent advancements in the fabrication and photocatalytic applications of graphitic carbon nitride–tungsten oxide nanocomposites", *Nanoscale Advances*, 5(19), 5214–5255, 2023. https://doi.org/10.1039/d3na00159h.

[7] J. Y. Zheng, Q. Sun, J. Cui, X. Yu, S. Li, L. Zhang, S. Jiang, W. Ma, R. Ma, "Review on recent progress in WO_3-based electrochromic films: preparation methods and performance enhancement strategies", *Nanoscale*, 15(1), 63–79, 2022. https://doi.org/10.1039/d2nr04761f.

[8] M. Epifani, "Mechanistic insights into WO_3 sensing and related perspectives", *Sensors*, 22(6), 2247, 2022. https://doi.org/10.3390/s22062247.

[9] S. Poongodi, P. S. Kumar, D. Mangalaraj, P. Nagamony, P. Meena, Y. Masuda, C. Lee, "Electrodeposition of WO_3 nanostructured thin films for electrochromic and H_2S gas sensor applications", *Journal of Alloys and Compounds*, 719, 71–81, 2017. https://doi.org/10.1016/j.jallcom.2017.05.122.

[10] T. Xiang, Q. Xu, H. Liu, Y. Lu, "A high-performance electrochromic Mo-doped WO_3 film towards smart window", *Journal of Physics: Conference Series*, 3009(1), 012018, 2025. https://doi.org/10.1088/1742-6596/3009/1/012018.

[11] X. Sun, D. Wang, W. Wu, X. Zhao, X. Zhang, B. Wang, X. Rong, G. Wu, X. Wang, "Amorphous and crystalline Ti-doped $WO_3{\cdot}2H_2O$ for dual-band electrochromic smart windows", *ACS Sustainable Chemistry & Engineering*, 12(14), 5459–5467, 2024. https://doi.org/10.1021/acssuschemeng.3c07679.

[12] H. Zhao, X. Yu, S. Yu, H. Yang, W. Guo, S. Li, J. Y. Zheng, "Review on amorphous WO3 for electrochromic devices: structure, optimization strategies and applications", *Materials Today Chemistry*, 43, 102513, 2025. https://doi.org/10.1016/j.mtchem.2025.102513.

[13] International Energy Agency, "Global Hydrogen Review 2025", Paris, France, 2025. https://www.iea.org/reports/global-hydrogen-review-2025.

[14] C. G. Granqvist, "Electrochromics for smart windows: oxide-based thin films and devices", *Thin Solid Films*, 564, 1–38, 2014. https://doi.org/10.1016/j.tsf.2014.02.002.

[15] J. Cen, Q. Wu, D. Yan, W. Zhang, Y. Zhao, X. Tong, M. Liu, A. Orlov, "New aspects of improving the performance of WO_3 thin films for photoelectrochemical water splitting by tuning the ultrathin depletion region", *RSC Advances*, 9(2), 899–905, 2019. https://doi.org/10.1039/c8ra08875f.

[16] H. Habazaki, Y. Hayashi, H. Konno, "Characterization of electrodeposited WO_3 films and its application to electrochemical wastewater treatment", *Electrochimica Acta*, 47(26), 4181–4188, 2002. https://doi.org/10.1016/S0013-4686(02)00435-8.

[17] M. Murtaza, W. A. Shah, A. Waseem, "WO_3/Nb_2CTx MXene 2D–2D heterojunction as a high performance photoanode for photoelectrochemical water splitting", *Nanoscale Advances*, 7(14), 4450–4460, 2025. https://doi.org/10.1039/d5na00345h.

[18] J. Zhang, C. D. Van, K. Takei, M. H. Lee, "Three-dimensional WO_3 nanorod arrays on Si as photoanodes for efficient photoelectrochemical water splitting", *Journal of Industrial and Engineering Chemistry*, 124, 550–557, 2023. https://doi.org/10.1016/j.jiec.2023.05.011.

[19] International Energy Agency, "World Energy Outlook 2025", Paris, France, 2025. https://www.iea.org/reports/world-energy-outlook-2025.

[20] J. Guo, H. Jia, Z. Shao, P. Jin, X. Cao, "Fast-switching WO_3-based electrochromic devices: design, fabrication, and applications", *Accounts of Materials Research*, 4(5), 438–447, 2023. https://doi.org/10.1021/accountsmr.2c00217.

[21] M. G. Walter, E. L. Warren, J. R. McKone, S. W. Boettcher, Q. Mi, E. A. Santori, N. S. Lewis, "Solar water splitting cells", *Chemical Reviews*, 110(11), 6446–6473, 2010. https://doi.org/10.1021/cr1002326.

[22] S. J. Hong, S. Lee, J. S. Jang, J. S. Lee, "Heterojunction $BiVO_4/WO_3$ electrodes for enhanced photoactivity of water oxidation", *Energy & Environmental Science*, 4(5), 1781–1787, 2011. https://doi.org/10.1039/c0ee00743a.

[23] M. E. Orazem, B. Tribollet, *Electrochemical Impedance Spectroscopy*, 2nd ed., Hoboken, NJ, USA, Wiley, 2017.

[24] J. Bisquert, S. Giménez, L. Bertoluzzi, I. Herraiz-Cardona, "Analysis of photoelectrochemical systems by impedance spectroscopy", *Photoelectrochemical Solar Fuel Production*, S. Giménez, J. Bisquert (Eds.), Cham, Switzerland, Springer, 2016, Ch. 6, 281–321. https://doi.org/10.1007/978-3-319-29641-8.

[25] E. Barsoukov, J. R. Macdonald, *Impedance Spectroscopy: Theory, Experiment, and Applications*, 3rd ed., Hoboken, NJ, USA, Wiley, 2018.

[26] E. A. Ponomarev, L. M. Peter, "A comparison of intensity modulated photocurrent spectroscopy and photoelectrochemical impedance spectroscopy in a study of photoelectrochemical hydrogen evolution at p-InP", *Journal of Electroanalytical Chemistry*, 397(1-2), 45–52, 1995. https://doi.org/10.1016/0022-0728(95)04148-9.

[27] T. Hisatomi, J. Kubota, K. Domen, "Recent advances in semiconductors for photocatalytic and photoelectrochemical water splitting", *Chemical Society Reviews*, 43(22), 7520–7535, 2014. https://doi.org/10.1039/c3cs60378d.

[28] D. Klotz, D. A. Grave, H. Dotan, A. Rothschild, "Empirical analysis of the photoelectrochemical impedance response of hematite photoanodes for water photo-oxidation", *Journal of Physical Chemistry Letters*, 9(6), 1466–1472, 2018. https://doi.org/10.1021/acs.jpclett.8b00096.

[29] B. Klahr, T. Hamann, "Water oxidation on hematite photoelectrodes: insight into the nature of surface states through in situ spectroelectrochemistry", *The Journal of Physical Chemistry C*, 118(19), 10393–10399, 2014. https://doi.org/10.1021/jp500543z.

[30] X. Shi, I. Herraiz-Cardona, L. Bertoluzzi, P. Lopez-Varo, J. Bisquert, J. H. Park, S. Gimenez, "Understanding the synergistic effect of WO_3–$BiVO_4$ heterostructures by impedance spectroscopy", *Physical Chemistry Chemical Physics*, 18(13), 9255–9261, 2016. https://doi.org/10.1039/c5cp07905e.

[31] M. Fox, *Optical Properties of Solids*, Oxford, 2nd Ed., United Kingdom: Oxford University Press, 2010.

[32] Z. Zhang, H. Chen, Z. Lin, X. Guan, J. Zhang, X. Tang, Y. Zhan, J. Luo, "Pivotal role of the granularity uniformity of the WO_3 film electrode upon the cyclic stability during cation insertion/extraction", *Nanomaterials*, 13(6), 973, 2023. https://doi.org/10.3390/nano13060973.

[33] K. Ç. Demir, "Corrosion behavior of electrodeposited WO_3 thin films", *Ceramics International*, 46(4), 4358–4364, 2020. https://doi.org/10.1016/j.ceramint.2019.10.159.

[34] G. Leftheriotis, P. Yianoulis, "Development of electrodeposited WO_3 films with modified surface morphology and improved electrochromic properties", *Solid State Ionics*, 179(38), 2192–2197, 2008. https://doi.org/10.1016/j.ssi.2008.07.018.

[35] W. L. Kwong, N. Savvides, C. C. Sorrell, "Electrodeposited nanostructured WO_3 thin films for photoelectrochemical applications", *Electrochimica Acta*, 75, 371–380, 2012. https://doi.org/10.1016/j.electacta.2012.05.019.

[36] G. Mineo, F. Ruffino, S. Mirabella, E. Bruno, "Investigation of WO_3 electrodeposition leading to nanostructured thin films", *Nanomaterials*, 10(8), 1493, 2020. https://doi.org/10.3390/nano10081493.

[37] W. L. Kwong, H. Qiu, A. Nakaruk, P. Koshy, C. C. Sorrell, "Photoelectrochemical properties of WO_3 thin films prepared by electrodeposition", *Energy Procedia*, 34, 617–626, 2013. https://doi.org/10.1016/j.egypro.2013.06.793.

[38] H. D. Zheng, J. Z. Ou, M. S. Strano, R. B. Kaner, A. Mitchell, K. Kalantar-Zadeh, "Nanostructured tungsten oxide—properties, synthesis, and applications", *Advanced Functional Materials*, 21(12), 2175–2196, 2011. https://doi.org/10.1002/adfm.201002477.

[39] J. Liu, G. Zhang, K. Guo, D. Guo, M. Shi, H. Ning, T. Qiu, J. Chen, X. Fu, R. Yao, J. Peng, "Effect of the ammonium tungsten precursor solution with the modification of glycerol on wide band gap WO_3 thin film and its electrochromic properties", *Micromachines*, 11(3), 311, 2020. https://doi.org/10.3390/mi11030311.